nature chemistry

Article

https://doi.org/10.1038/s41557-023-01160-x

Isolation, bonding and reactivity of a monomeric stibine oxide

Received: 11 January 2022

Accepted: 14 February 2023

John S. Wenger[1], Monica Weng[2], Graham N. George[2,3] & Timothy C. Johnstone[1]

In contrast to phosphine oxides and arsine oxides, which are common and exist as stable monomeric species featuring the corresponding pnictoryl functional group ($Pn{=}O/Pn^{+}{-}O^{-}$; Pn = P, As), stibine oxides are generally polymeric, and the properties of the unperturbed stiboryl group ($Sb{=}O/Sb^{+}{-}O^{-}$) remain unexplored. We now report the isolation of the monomeric stibine oxide, $Dipp_3SbO$ (where Dipp = 2,6-diisopropylphenyl). Spectroscopic, crystallographic and computational studies provide insight into the nature of the $Sb{=}O/Sb^{+}{-}O^{-}$ bond. Moreover, isolation of $Dipp_3SbO$ allows the chemistry of the stiboryl group to be explored. Here we show that $Dipp_3SbO$ can act as a Brønsted base, a hydrogen-bond acceptor and a transition-metal ligand, in addition engaging in 1,2-addition, O-for-F_2 exchange and O-atom transfer. In all cases, the reactivity of $Dipp_3SbO$ differed from that of the lighter congeners $Dipp_3AsO$ and $Dipp_3PO$.

The stability of the pnictogen–oxygen bond in phosphine oxides has been used for over a century to drive chemical reactions such as those discovered by Wittig[1], Mitsunobu[2], Appel[3] and Staudinger[4]. The electronic structure that gives rise to the stability of the $P{=}O/P^{+}{-}O^{-}$ bond was once a topic of intense debate, but the currently accepted model features a single covalent bond between the P and O atoms strengthened by electrostatic attraction between the P^{+} and O^{-} centres as well as donation from O-centred lone pairs into P–C antibonding orbitals[5]. As the Group 15 element increases in atomic number, however, the pnictogen valence orbitals become more diffuse, overlap with O-based orbitals decreases, and the pnictogen atom becomes increasingly able to expand its coordination sphere. These trends suggest that the heavier congeners of phosphine oxides could exhibit distinct and interesting reactivity[6]. The behaviour and properties of these heavier congeners would also provide a means of validating the bonding model currently used to describe the $Pn{=}O/Pn^{+}{-}O^{-}$ bond, where Pn is a pnictogen[5]. For As, the variations from P are small enough, possibly as a result of the scandide contraction[7], that arsine oxides are generally analogous to phosphine oxides: they are monomeric species with $As{=}O/As^{+}{-}O^{-}$ polar covalent bonds. For example, oxidation of either Ph_3P or Ph_3As with H_2O_2 readily affords monomeric Ph_3PnO (Pn = P, As; Fig. 1a). The situation changes substantially for Sb: no molecules containing an unperturbed $Sb{=}O/Sb^{+}{-}O^{-}$ bond have ever been isolated.

A substance described as triphenylstibine oxide was first reported in 1938[8], and many other investigators subsequently purported to produce 'Ph_3SbO' by treating Ph_3Sb with H_2O_2 (ref. [9]). Melting-point measurements and careful molecular-weight determinations showed these different substances to be dimeric or polymeric compounds and their structures were ultimately established with single-crystal X-ray diffraction and Sb extended X-ray absorption fine structure analysis (EXAFS; Fig. 1b)[10–12].

Although Ph_3SbO is not stable as a monomer, disaggregation of the polymer can be achieved with the Lewis acid $B(C_6F_5)_3$ to afford the Lewis acid–base adduct $Ph_3SbOB(C_6F_5)_3$ (Fig. 1d)[13]. Another Lewis-acid-stabilized stibine oxide was obtained with a biphenylene-bridged system featuring a stibine oxide intramolecularly coordinated to a stiborane (Fig. 1e)[14]. A final example of Lewis-acid stabilization comprises $[(3,5\text{-}F_2C_6H_3)_4SbOSbEt_3][B(C_6F_5)_4]$, which formed when a mixture of Et_3Sb and $[(3,5\text{-}F_2C_6H_3)_4Sb][B(C_6F_5)_4]$ was exposed to oxygen[15]. In these compounds, interaction with a Lewis acid stabilizes

---

[1]Department of Chemistry and Biochemistry, University of California Santa Cruz, Santa Cruz, CA, USA. [2]Department of Geological Sciences, University of Saskatchewan, Saskatoon, Saskatchewan, Canada. [3]Department of Chemistry, University of Saskatchewan, Saskatoon, Saskatchewan, Canada. e-mail: johnstone@ucsc.edu

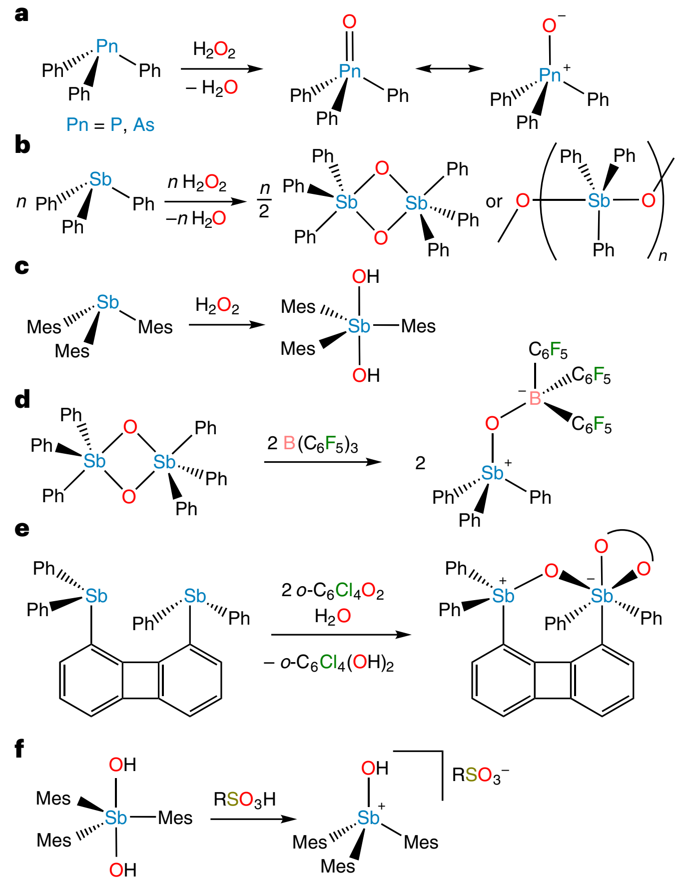

Fig. 1 | Synthesis of pnictine oxides. **a**, Oxidation of Ph_3Pn yields monomeric Ph_3PnO for Pn = P and As. **b**, Oxidation of Ph_3Sb yields dimers or polymers. **c**, Oxidation of Mes_3Sb yields *trans*-$Sb(OH)_2Mes_3$ (ref. [22]). **d**, Lewis-acid-mediated disaggregation of $(Ph_3SbO)_2$ (ref. [13]). **e**, Synthesis of an intramolecular stiborane-stabilized stibine oxide[14]. The chelating moiety (shown as a curved line) represents *o*-$C_6Cl_4O_2$. **f**, Treatment of *trans*-$Sb(OH)_2Mes_3$ with sulfonic acids yields a hydroxystibonium salt and not a stibine oxide.

the stibine oxide but also perturbs the Sb–O bonding interaction, preventing direct analysis of the periodic bonding trend across the pnictine oxides. These examples highlight that stibine oxides can be non-aggregated, but they raise the question of whether a monomeric stibine oxide is isolable in the absence of a Lewis acid interacting with and stabilizing the Sb=O/Sb$^+$–O$^-$ bond. Matrix isolation studies afford evidence for the existence of monomeric H_3SbO (Sb–O stretching frequency (ν_{SbO}) = 825 cm^{-1}), but only in solid argon at 12 K (ref. [16]).

We sought to explore a kinetic stabilization approach in which the reactive Sb=O/Sb$^+$–O$^-$ bond is protected by sterically bulky groups, a strategy that has been used with great success in the stabilization of other reactive main-group bonds[17–21]. The bulky mesityl groups of Mes_3Sb prevent polymerization upon treatment with H_2O_2, but not coordination sphere expansion: the product is the stiborane *trans*-$Sb(OH)_2Mes_3$ (Fig. 1c)[22]. Our re-investigation of reports of Mes_3SbO showed that the reported species is, in fact, a hydroxystibonium cation (Fig. 1f)[23,24]. This work similarly called into question the previously reported $(2,6\text{-}(MeO)_2Ph)_3SbO$ (ref. [25]).

Results

Synthesis and characterization

We sought to prepare the even more sterically hindered stibine $Dipp_3Sb$, **1a**, where Dipp = 2,6-diisopropylphenyl. Although many R_3Sb species are readily accessed from $SbCl_3$ and either RMgBr or RLi, these strategies do not afford **1a**. We therefore adapted a synthetic strategy developed by Sasaki and colleagues[26,27], whereby the aryl group is installed on the Sb centre with an organocopper(I) species. In this way, **1a** was isolated as a colourless, crystalline, air-stable solid (Fig. 2a). Although the ^{1}H NMR spectrum of **1a** indicates that rotation about the Sb–C and C_{Ar}–C_{iPr} bonds is rapid on the NMR timescale at room temperature, the X-ray crystal structure highlights the extremely crowded environment around the Sb atom (Fig. 2b,c). The corresponding arsine (**1b**) and phosphine (**1c**) were similarly prepared (Fig. 2).

Addition of **1a** to a suspension of PhIO in CH_2Cl_2 led to rapid consumption of the solid. Solvent was stripped from the reaction mixture and the residue was washed with pentane to yield a colourless solid, **2a** (Fig. 3a). The infrared spectrum of **2a** shows a new band at 779 cm^{-1}, which we assign as a ν_{SbO} stretching frequency. This value is greater than any of the ν_{SbO} values of $(Ph_3SbO)_2$ (643/651 cm^{-1})[10], *trans*-$Sb(OH)_2Mes_3$ (520 cm^{-1})[22,28] or $[Mes_3SbOH][O_3SPh]$ (612 cm^{-1})[23]. The ^{1}H NMR spectrum of **2a** is distinct from that of **1a** and is consistent with a single Dipp environment with restricted rotation about the Sb–C bonds. Exchange spectroscopy (EXSY) and variable temperature (VT) NMR experiments confirmed the chemical exchange and reversible resonance coalescence (Supplementary Figs. 17 and 18).

The oxidation state of **2a** was probed with Sb X-ray absorption spectroscopy (XAS), which we have recently used to shed light on the structures of Sb-containing compounds[29]. The Sb K edge of **2a** is 2 eV higher in energy than that of **1a** (Fig. 3c). A similar shift was seen for a variety of Sb(V) compounds, including a dimeric stibine oxide $(Ph_3SbO)_2$ (**A**), a dihydroxystiborane *trans*-$Sb(OH)_2Mes_3$ (**B**) and a hydroxystibonium salt $[Dipp_3SbOH][O_3SPh]$ (**C**, vide infra), indicating that **2a** also contains Sb(V) (Fig. 3c). The K-edge EXAFS data were collected to high resolution to gain further insight into the structure of **2a**. Similar data were collected from **1a**, **A**, **B** and **C** for comparison (Fig. 3d). The Fourier transform of the data from **A** shows a distinct Sb···Sb scattering at 3.148(3) Å (superimposed on an outer-shell carbon backscattering), which is absent for **B** and **C** as well as **2a**, indicating that **2a** does not feature a dioxadistibetane. A detailed fit of the data from **B** shows two O scatters at 2.128(3) Å, whereas **C** is better fit by a single O scatterer at 1.905(1) Å. These values are in excellent agreement with the crystallographically determined structures of these compounds. In contrast, the data from **2a** are best fit with a single

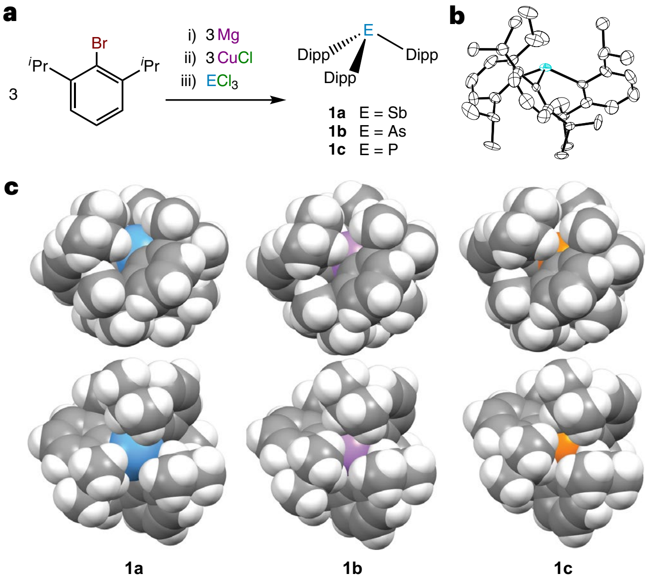

Fig. 2 | Synthesis of sterically crowded pnictines 1a–c. **a**, Synthesis of **1a**–**c**, Dipp = 2,6-diisopropylphenyl. **b**, Thermal ellipsoid diagram of **1a** at the 50% probability level, with H atoms omitted for clarity. **c**, Space-filling diagrams of **1a**–**c** from views rotated by 90° about the horizontal axis. Colour code: Sb, teal; As, purple; P, orange; C, grey; H, white.

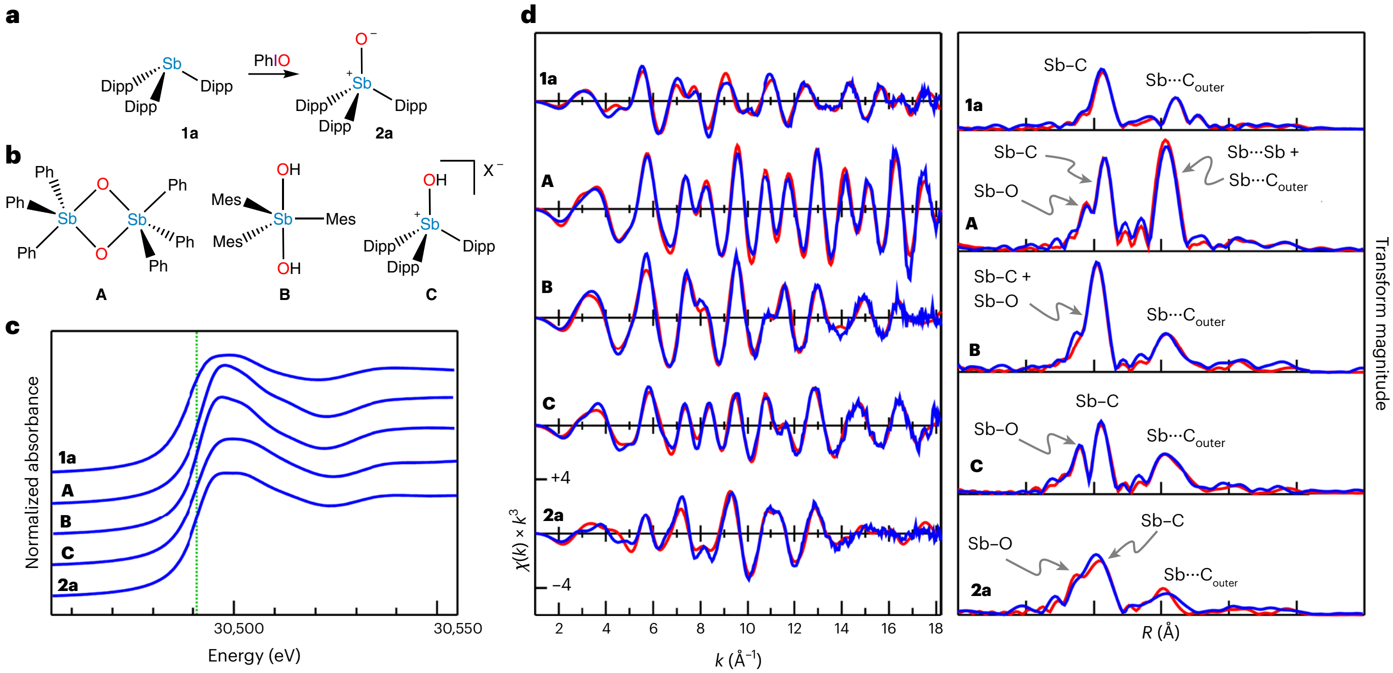

Fig. 3 | Oxidation of sterically crowded stibine 1a. a, Oxidation of **1a** with PhIO to give **2a**. **b**, Model compounds featuring different Sb–O bonding motifs. **A**, A dimeric stibine oxide; **B**, a dihydroxystiborane; **C**, a hydroxystibonium salt with X = O_3SPh. **c**, Sb K-edge XAS spectra, with a green dotted line indicating where the derivative is maximal for **2a**. Full normalized Sb K-edge XAS spectra are provided in Supplementary Fig. 109. **d**, Sb K-edge EXAFS (left) and Sb–C phase-corrected Fourier transforms (right). Experimental data are shown in blue and fits in red. The relevant EXAFS parameters are provided in Supplementary Table 7. A breakdown of the contributions of the different scatterers to the EXAFS and Sb–C phase-corrected Fourier transforms of **A** and **2a** are shown in Supplementary Figs. 110 and 111, respectively.

O-atom scatterer at a distance of 1.837(2) Å, which is substantially shorter than the Sb–O bonds characterized for any other isolated materials. Fit of a C atom in the place of the short Sb–O gave a worse goodness-of-fit index (F = 0.335 for Sb–C versus 0.319 for Sb–O) and a physically unreasonable Debye–Waller factor (σ^2 = 0.0010 Å^2 for Sb–C versus 0.0021 Å^2 for Sb–O).

Ultimately, we were successful in growing diffraction-quality single crystals of **2a**. The asymmetric unit of the crystal structure features a single molecule of $Dipp_3SbO$, which we unambiguously assign as the identity of **2a** (Fig. 4a). Hirshfeld atom refinement (HAR) afforded a Sb–O bond length of 1.8372(5) Å, which is in excellent agreement with the EXAFS distance. The next-nearest Sb···O distance is 9.0791(4) Å; space-filling diagrams highlight the steric shielding provided by the Dipp groups (Supplementary Fig. 99). One of the ^{i}Pr C–H units is directed at the stiboryl O atom with an O···H distance of 2.132(9) Å (note: HAR affords freely refined H-atom positions similar to those given by neutron diffraction)[30]. The C–H···O bond angle of 148.1(8)° suggests a strong electrostatic contribution to the interaction relative to weaker C–H···O H-bonds, in which isotropic van der Waals forces play a larger role[31].

The molecular geometry of **2a** from our X-ray crystal structure is in excellent agreement with the one from a theoretical geometry optimization (PBE0/def2-TZVPP), which features an Sb–O bond length of 1.827 Å. Notably, the scaled theoretical ν_{SbO} of 781 cm^{-1} at the gas-phase optimized geometry is in excellent agreement with the experimental value for **2a** (779 cm^{-1}). These results combine to allow us to conclude that we have isolated an example of a monomeric stibine oxide. For comparison, we similarly synthesized and characterized the lighter congeners $Dipp_3AsO$ (**2b**) and $Dipp_3PO$ (**2c**).

Electronic structure

To gain insight into the nature of the Sb=O/Sb$^+$–O$^-$ bonding motif, we analysed the topology of the theoretical electron density of **2a** (DKH-PBE0/old-DKH-TZVPP) (Fig. 4c–e). This analysis shows the locations of critical points in the electron density (ρ), that is, points in space where the derivative of ρ is zero in three mutually orthogonal directions. These critical points are characterized with a pair of numbers (ω, σ), where ω is the number of non-zero eigenvalues of the Hessian and σ is the sum of the signs of those eigenvalues[32]. As expected, a (3, −3) critical point is present near the nuclear position of each atom. We also identified (3, −1) critical points, also known as bond critical points, between each of the covalently bonded atoms (Supplementary Fig. 76). Although the values of various real-space functions at a (3, −1) critical point are frequently used to describe the nature of that bonding interaction[32], for polar covalent bonds, like the Sb$^+$–O$^-$ bond in a stibine oxide, these functions are more informative when evaluated along the length of the bond path (Fig. 4e)[33]. For the Sb–O bond of **2a**, ρ features a single minimum at 0.173 e$^-$Å^{-3}, approximately halfway along the bond path. In the valence bonding region, the Laplacian ($\nabla^2\rho$) exhibits a single O-proximal minimum of −1.346 e$^-$Å^{-5}. The ellipticity (ε) is negligible along the length of the bond path. The decrease in ρ and $|\nabla^2\rho|$ in the internuclear space from **2c** to **2b** to **2a** suggests a systematic weakening of the Pn$^+$–O$^-$ bond as the Group 15 element increases in atomic number. We note that the topological analysis also located bond paths connecting the pnictoryl O atoms and the ^{i}Pr C–H units, as suggested by the crystallographic data. The analysis of the bond critical points of these interactions (Supplementary Tables 12 and 13) indicates that hydrogen-bonding interactions are present and that they decrease in magnitude from **2a** to **2b** to **2c**.

Further insight into the Sb–O bonding in **2a** was obtained from molecular orbital analyses. The canonical molecular orbitals (CMOs) are, as expected, highly delocalized across the molecule (Fig. 5b). The frontier CMOs feature substantial π or π* character from the Dipp substituents. The nearly degenerate highest occupied molecular orbital (HOMO) and HOMO−1 feature a substantial contribution from the lone pairs on the O atom. The lowest unoccupied molecular orbital

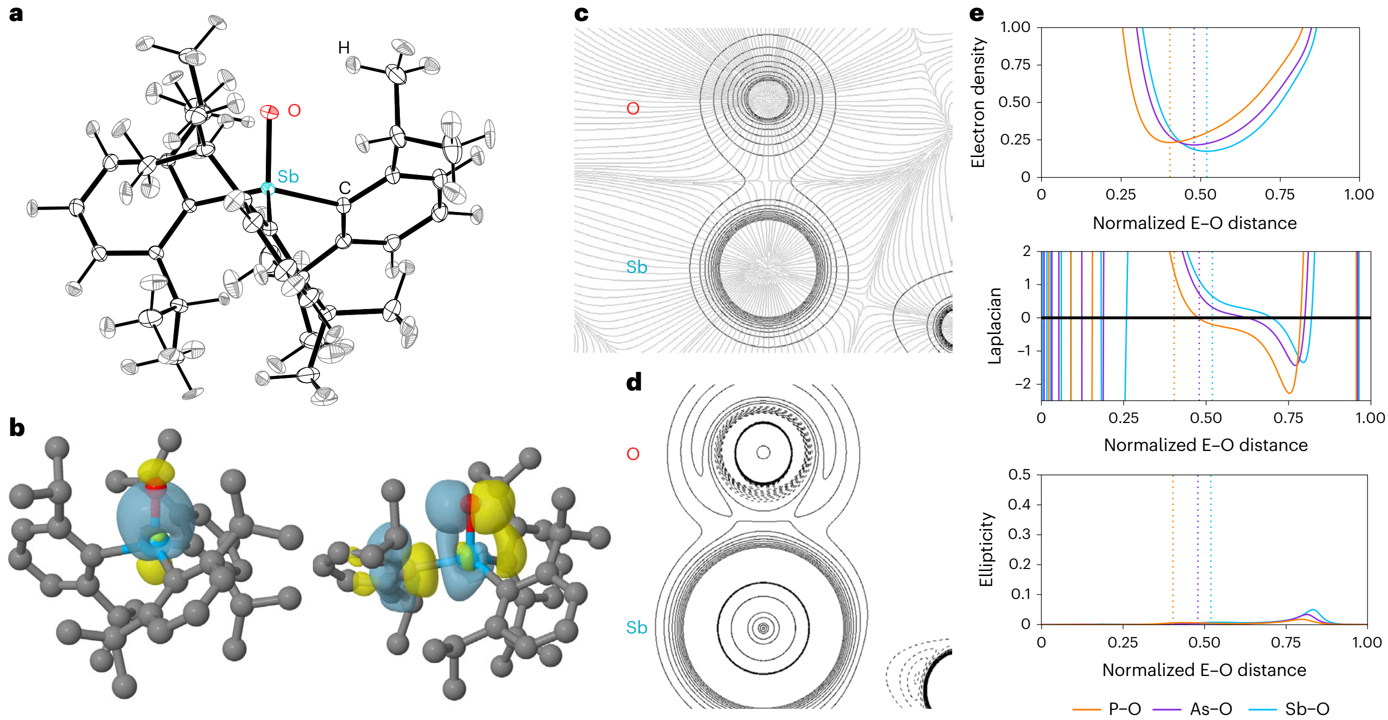

Fig. 4 | The structure and bonding of 2a, a monomeric stibine oxide. **a**, Thermal ellipsoid plot of **2a** at the 50% probability level. Colour code: Sb, teal; O, red; C, black; H, grey. **b**, Surface plots (isovalue = 0.05) depicting the Sb–O bonding NLMO (left) and overlap of O lone pair and Sb–C antibonding pre-orthogonalized NLMOs (right). Colour code: Sb, teal; O, red; C, grey; H, white. **c**, Contour plot of ρ overlaid with the gradient field lines of ρ for the Sb–O bond. **d**, Contour plot of $\nabla^2\rho$ for the Sb–O bond, with positive values contoured with solid lines and negative values with dashed lines. **e**, Values of ρ ($e^- Å^{-3}$), $\nabla^2\rho$ ($e^- Å^{-5}$) and ellipticity ε for **2a**–**c** along the Pn–O bond paths, with Pn at the left and O at the right along the horizontal axis. The bond length is normalized to 1.00. The location of the (3, −1) critical point is shown with a dashed vertical line.

(LUMO) features a substantial amount of Sb–O σ^* character. The Dipp groups block the lobe of this orbital that extends opposite the Sb–O bond, which probably contributes to the stability of this molecule, as designed.

More detailed information was obtained by analysing the natural localized molecular orbitals (NLMOs) of **2a** (Fig. 4b and Supplementary Figs. 91–93). An Sb–O bonding NLMO is present and is polarized 74:25 toward the more electronegative O atom, which uses a hybrid atomic orbital enriched in *p* character (79%) to interact with the Sb. The Sb–O antibonding orbital is correspondingly polarized toward the Sb and exhibits the large lobe opposite the Sb–O bond that was observed in the LUMO CMO. There are two O-centred lone pair natural bond orbitals (NBOs) with nearly pure *p* character and a second-order perturbation theory analysis uncovered donor–acceptor interactions that delocalize electron density from these lone pairs into Sb–C antibonding orbitals (Supplementary Table 14). Similar delocalizations were observed for **2b** and **2c**, and deletion calculations showed that the non-covalent interactions between the O and $Dipp_3Pn$ fragments decreased from **2c** to **2b** to **2a**. These donor–acceptor interactions strengthen the Pn–O bonds, and the decreased delocalization in **2a** affords the lowest Wiberg Pn–O bond order of the three, but the O atom consequently retains the greatest natural atomic charge (Supplementary Table 15). The variation in charge accumulation is also reflected in the magnitude of the electrostatic surface potential minimum, for which **2c** < **2b** < **2a** (Fig. 5c). The decrease in $Pn^+–O^-$ bond strength (PO > AsO > SbO), is also reflected in the $Pn^+–O^-$ stretch force constants (Supplementary Fig. 75) and the ratio of $\Delta E_{orb}/\Delta E_{total}$ from an energy decomposition analysis of O and $Dipp_3Pn$ fragments (Supplementary Tables 8–10). Deformation density analyses show a redistribution of electron density from the $Dipp_3Pn$ fragment to the O atom to an extent that decreases from Sb to As to P (Supplementary Fig. 90).

Donor–acceptor interactions were also observed from the O-centred lone pairs to the ^{i}Pr C–H antibonding orbitals for **2a**–**c** (Supplementary Fig. 93), consistent with the presence of the O⋯H bond paths noted above. Non-covalent interaction analysis of **2a** (Supplementary Fig. 89) uncovered a region with a negative product of ρ and the sign of the second-largest eigenvalue of the Hessian of ρ, sign(λ_2)ρ, between the O and ^{i}Pr C–H; the value of sign(λ_2)ρ was less negative for **2b** and **2c**, indicating that this interaction, which may help to stabilize the $Sb^+–O^-$ bond, is present in **2a** and weakens for **2b** and **2c**. The presence of this hydrogen-bonding interaction in **2a** was further confirmed by NBO perturbation theory and deletion calculations (Supplementary Fig. 93).

Reactivity

With an isolated stibine oxide in hand, we next explored its chemistry. The bonding characteristics outlined above suggest that **2a** should exhibit O-centred Lewis-basic behaviour. Cooling a solution of **2a** in neat 4-fluoroaniline affords colourless blocks, which X-ray diffraction analysis confirmed to contain the stibine oxide-aniline hydrogen-bonded adduct **3** (Fig. 6(i)). In the HAR model, the hydrogen-bonding H atom of **3** is located on the N atom with a N–H distance of 1.04(2) Å. The N⋯O distance of 2.858(1) Å implies that the hydrogen-bonding interaction is of moderate strength. The Sb–O bond remains short at 1.8421(7) Å, but is statistically significantly lengthened as compared to **2a**. Consistent with this bond lengthening, the Sb–O IR stretching frequency decreases slightly from 779 cm^{-1} for **2a** to 762 cm^{-1} for **3**. Neither **2b** nor **2c** affords a similar product, consistent with the lower nucleophilicity of the O atoms in these species.

We next sought to determine whether this Lewis basicity would also manifest in metal ion coordination. Combination of **2a** with 1 equiv. of CuCl yielded the complex $(Dipp_3SbO)CuCl$ (**4**; Fig. 6(ii)),

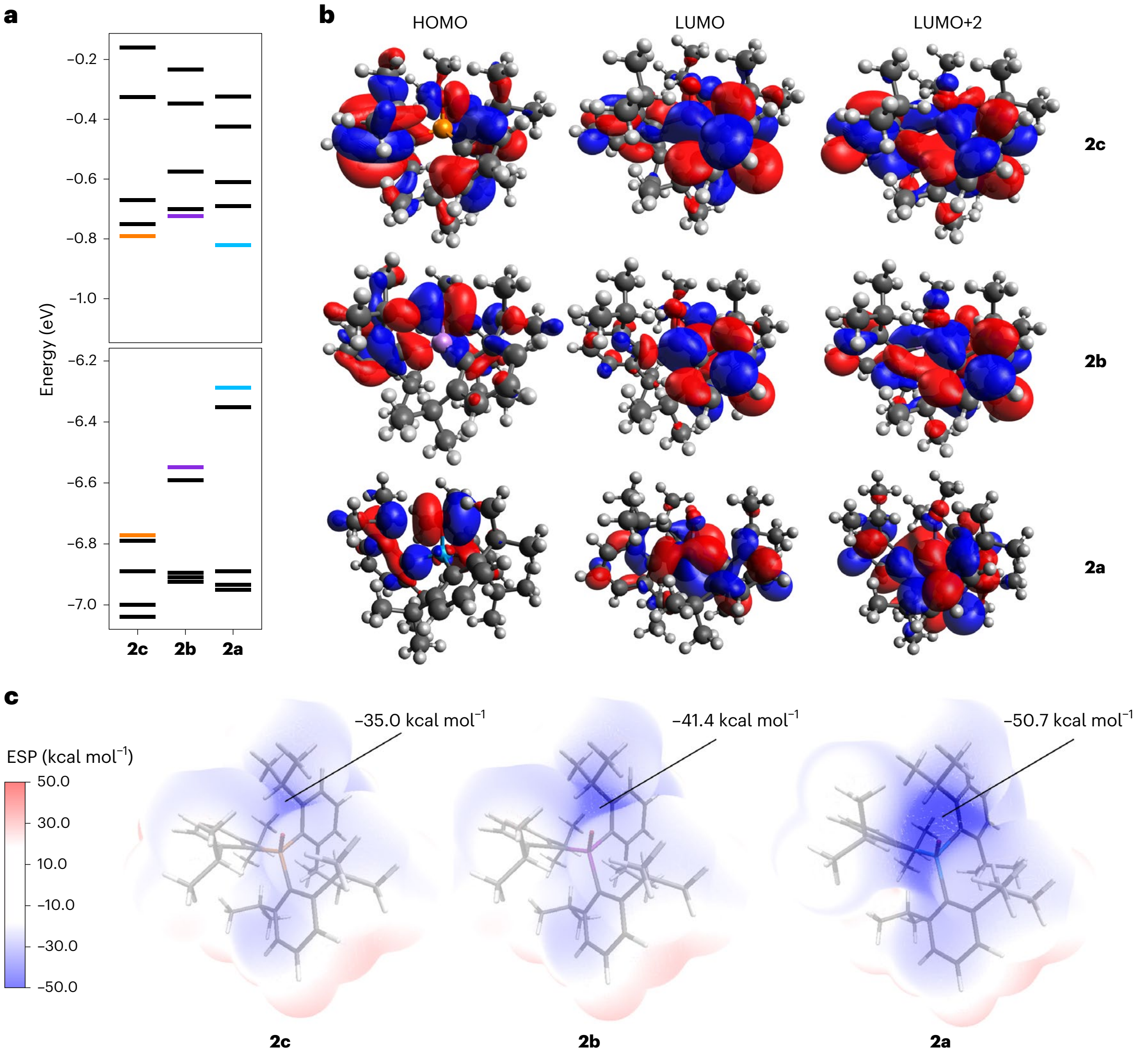

Fig. 5 | Variation in the electronic structure of the pnictine oxides 2a–c. **a**, Calculated orbital energies (DKH-PBE0/old-DKH-TZVPP//PBE0/def2-TZVPP) in electronvolts, with frontier molecular orbitals shown in colour (P, orange; As, purple; Sb, teal). **b**, Canonical molecular orbital diagrams of **2c**, **2b** and **2a**. Colour code surfaces: red, positive; blue, negative (isovalue = 0.02). **c**, Electrostatic surface potential (ESP) mapped van der Waals surfaces of **2c**–**a** (values in kcal mol^{-1}). The value of the surface minimum is indicated. C, grey; H, white; O, red; P, orange; As, purple; Sb, teal.

whereas combination with 0.5 equiv. of AgOTf yielded [(Dipp$_3$SbO)$_2$Ag][OTf] (**5**; Fig. 6(iii)). If ClAu(PPh$_3$) was treated with AgOTf and **2a**, the salt [(Dipp$_3$SbO)Au(PPh$_3$)][OTf] (**6**; Fig. 6(iv)) was isolated. All three of the complexes were crystallographically characterized, and all three exhibit significantly nonlinear Sb–O–M angles (Supplementary Table 18). Solution of the structure of a second polymorph of **6** showed, however, that the complex can also take on a rigorously linear configuration. The Sb–O–M bending is most probably driven by crystal packing forces. We note that, in all cases, the geometry about the metal centres in **4**–**6** is nearly perfectly linear, as expected. Neither **2b** nor **2c** was able to form analogous complexes; the NMR resonances of these lighter pnictine oxides exhibited only minor shifts upon mixing with the metal precursors (Supplementary Fig. 49–51). We note that the strength of the intramolecular CH$_{iPr}$···O interaction decreases upon coordination of **2a** (Supplementary Tables 13 and 15).

Room-temperature treatment of **2a** with a strong Brønsted acid, PhSO$_3$H, resulted in clean formation of the hydroxystibonium salt [Dipp$_3$Sb(OH)][O$_3$SPh] (**7a**; Fig. 6(v)). Crystallographic analysis of the salt confirmed protonation at the Sb-bound O atom, which lengthens the Sb–O bond to 1.9119(7) Å and decreases ν_{SbO} to 611 cm^{-1}. Compound **2b** can be similarly protonated to yield [Dipp$_3$As(OH)][O$_3$SPh] (**7b**; Supplementary Fig. 106). Compound **2c** interacts much more weakly with PhSO$_3$H, but titration with up to 10 equiv. of the acid results in a systematic shift in the NMR resonances of **2c**. This behaviour may arise from reversible formation of a hydrogen-bonded adduct in equilibrium with the dissociated species (Supplementary Figs. 59 and 60).

We were surprised to find that, in contrast, acetic acid not only protonates the O atom of **2a**, but adds across the Sb–O bond at room temperature, affording the neutral stiborane *cis*-Sb(OH)(OAc)Dipp$_3$ (**8**; Fig. 6(vi)). This 1,2-addition chemistry highlights the unsaturated nature of the stiboryl (Sb=O/Sb$^+$–O$^-$) group. The *cis* isomer forms despite the expectation that the more sterically bulky Dipp groups would assume the less-crowded equatorial positions and that the more apicophilic hydroxy and acetoxy groups would assume the *trans*-disposed axial positions. An intramolecular hydrogen-bonding interaction is present between the hydroxy and acetoxy groups (O···O = 2.630(2) Å), which may be responsible for the *cis* configuration. Neither **2b** nor **2c** reacts in this manner with acetic acid (Supplementary Figs. 64–66). We have yet to observe any cycloaddition chemistry (Supplementary Fig. 74), but substrates continue to be explored.

Combination of **2a** and BF$_3$·OEt$_2$ at −78 °C results in rapid and clean conversion to **9**, which does not feature an ^{11}B NMR signal, but does exhibit a single sharp ^{19}F resonance at −74.35 ppm. X-ray diffraction analysis shows **9** to be the difluorostiborane *trans*-SbF$_2$Dipp$_3$

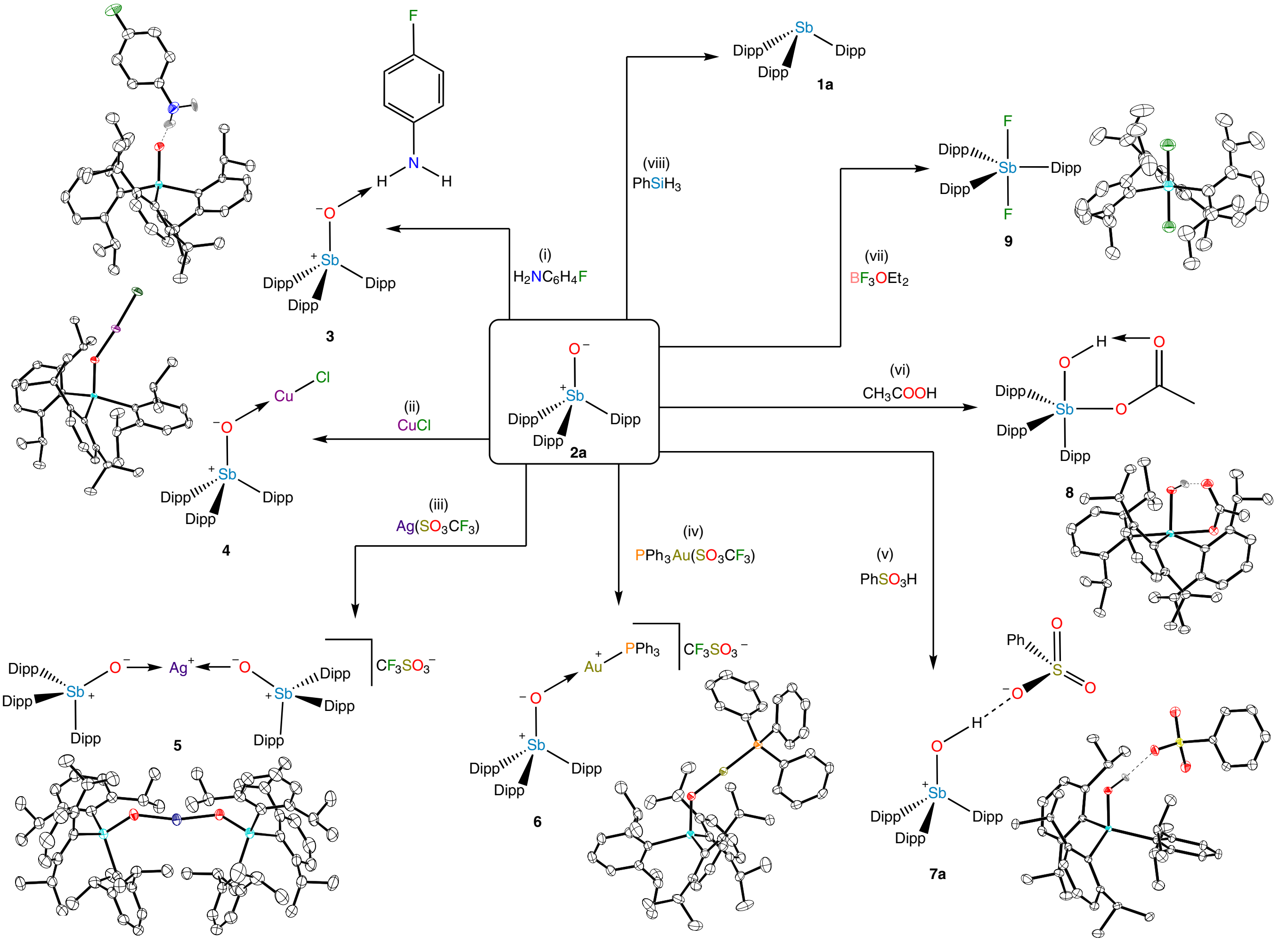

Fig. 6 | Reactivity of the stibine oxide 2a. (i) Reaction with an aniline to form a hydrogen-bonded adduct. (ii–iv) Reactions with copper(I) chloride, silver(I) triflate and triphenylphosphinegold(I) triflate to yield transition-metal coordination complexes. (v) Reaction with a sulfonic acid to yield a hydroxystibonium salt. (vi) Reaction with acetic acid to yield a *cis*-hydroxyacetatostiborane. (vii) Reaction with BF_3 to yield a *trans*-difluorostiborane. (viii) Reaction with phenylsilane to yield stibine **1a**. Thermal ellipsoid plots at the 50% probability level are shown next to products; non-polar H atoms are omitted for clarity. Sb, teal; O, red; C, black; H, grey; N, blue; Ag, purple; F, green; S, yellow; Au, gold; P, orange; Cu, mauve.

(Fig. 6(vii)). This reaction is the first in which we have observed cleavage of the Sb–O bond. The maintenance of the 5+ oxidation state of the Sb centre suggests that the reaction is an oxide transfer in which one oxide is exchanged for two fluoride groups, consistent with the fluorophilicity of organoantimony(V) Lewis acids[34]. We have not fully characterized the by-product, but boranes are known to form stable boroxines with O^{2-} (ref. [35]). Unlike **8**, **9** features the apicophilic fluoro substituents in the expected *trans* geometry (Sb–F = 1.9673(34) and 1.9706(31) Å), most probably as a result of the increased electronegativity of F and a lack of hydrogen bonding. No deoxygenation was observed upon combination of **2b** or **2c** with $BF_3{\cdot}OEt_2$.

Finally, we observed that $PhSiH_3$ is able to abstract the O atom from **2a** to cleanly afford **1a** (Fig. 6(viii)). The reaction does not proceed at room temperature, but readily reaches completion within 1 h at 50 °C. Under these mild conditions, neither **2b** nor **2c** reacts with $PhSiH_3$ (Supplementary Figs. 72 and 73).

Discussion

The isolation of a monomeric stibine oxide, **2a**, was achieved using a kinetic stabilization approach in which the unsaturated $Sb^+–O^-$ bond is protected by the sterically bulky Dipp groups bound to the Sb centre. The isolation of **2a** has permitted the spectroscopic and crystallographic characterization of this functional group. In combination with these experimental measurements, theoretical calculations provide insight into the nature of the Pn–O bonding interaction, and the variation in this bonding as the pnictogen is varied from Sb to As to P. The increased accumulation of charge on the O atom confers upon **2a** reactivity that differs notably from that of **2b** and **2c**. We have described examples of **2a** acting as a hydrogen-bond acceptor, a transition-metal ligand and a Brønsted base. The unsaturated nature of the $Sb^+–O^-$ bond also allows it to engage in addition chemistry, as exemplified by the reaction with acetic acid. Finally, the Sb–O bond can be cleaved, either with maintenance of the Sb(V) oxidation state, as in the reaction with BF_3, or with reduction to Sb(III), as in the reaction with $PhSiH_3$. We will continue to investigate in greater depth each of these classes of reactions, and others, with an emphasis on comparing and contrasting the reactivity of stibine oxides with that of phosphine and arsine oxides.

Online content

Any methods, additional references, Nature Portfolio reporting summaries, source data, extended data, supplementary information, acknowledgements, peer review information; details of author contributions and competing interests; and statements of data and code availability are available at https://doi.org/10.1038/s41557-023-01160-x.

References

1. Wittig, G. & Schöllkopf, U. Über triphenyl-phosphin-methylene als olefinbildende Reagenzien (I. Mitteil.). *Chem. Ber.* **87**, 1318–1330 (1954).
2. Mitsunobu, O. & Yamada, M. Preparation of esters of carboxylic and phosphoric acid via quaternary phosphonium salts. *Bull. Chem. Soc. Jpn* **40**, 2380–2382 (1967).
3. Appel, R. Tertiary phosphane/tetrachloromethane, a versatile reagent for chlorination, dehydration, and P–N linkage. *Angew. Chem. Int. Ed.* **14**, 801–811 (1975).
4. Staudinger, H. & Meyer, J. Über neue organische Phosphorverbindungen III. Phosphinmethylenderivate und Phosphinimine. *Helv. Chim. Acta* **2**, 635–646 (1919).
5. Yang, T., Andrada, D. M. & Frenking, G. Dative versus electron-sharing bonding in N-oxides and phosphane oxides R_3EO and relative energies of the R_2EOR isomers (E=N, P; R=H, F, Cl, Me, Ph). A theoretical study. *Phys. Chem. Chem. Phys.* **20**, 11856–11866 (2018).
6. Lipshultz, J. M., Li, G. & Radosevich, A. T. Main group redox catalysis of organopnictogens: vertical periodic trends and emerging opportunities in group 15. *J. Am. Chem. Soc.* **143**, 1699–1721 (2021).
7. Huheey, J. E. & Huheey, C. L. Anomalous properties of elements that follow 'long periods' of elements. *J. Chem. Educ.* **49**, 227–230 (1972).
8. Mel'nikov, N. N. & Rokilskaya, M. S. The mechanism of the oxidation of organic compounds compounds by selenium dioxide. III. *J. Gen. Chem. USSR (Zhurnal Obshchei Khimii)* **8**, 834–838 (1938).
9. McEwen, W. E., Briles, G. H. & Schulz, D. N. Preparation and reactions of triphenylstibine oxide. *Phosphorus Relat. Group V Elem.* **2**, 147–153 (1972).
10. Bordner, J., Doak, G. O. & Everett, T. S. Crystal structure of 2,2,4,4-tetrahydro-2,2,2,4,4,4-hexaphenyl-1,3,2,4-dioxadistibetane (triphenylstibene oxide dimer) and related compounds. *J. Am. Chem. Soc.* **108**, 4206–4213 (1986).
11. Carmalt, C. J., Crossley, J. G., Norman, N. C. & Orpen, A. G. The structure of amorphous Ph_3SbO: information from EXAFS (extended X-ray absorption fine structure) spectroscopy. *Chem. Commun.* **1996**, 1675–1676 (1996).
12. Ferguson, G., Glidewell, C., Kaitner, B., Lloyd, D. & Metcalfe, S. Second determination of the structure of dimeric triphenylstibine oxide. *Acta Crystallogr. C* **43**, 824–826 (1987).
13. Kather, R. et al. Lewis-acid induced disaggregation of dimeric arylantimony oxides. *Chem. Commun.* **51**, 5932–5935 (2015).
14. Chen, C.-H. & Gabbaï, F. P. Coordination of a stibine oxide to a Lewis acidic stiborane at the upper rim of the biphenylene backbone. *Dalton Trans.* **47**, 12075–12078 (2018).
15. Coughlin, O. *Structural Manipulation of Organoantimony Cations for Tuneable Lewis Acidity and Reactivity of Palladium Organoantimony Complexes*. PhD thesis, Nottingham Trent Univ. (2021).
16. Andrews, L., Moores, B. W. & Fonda, K. K. Matrix infrared spectra of reaction and photolysis products of stibine and ozone. *Inorg. Chem.* **28**, 290–297 (1989).
17. Rivard, E. & Power, P. P. Multiple bonding in heavier element compounds stabilized by bulky terphenyl ligands. *Inorg. Chem.* **46**, 10047–10064 (2007).
18. Wang, Y. et al. Stabilization of elusive silicon oxides. *Nat. Chem* **7**, 509–513 (2015).
19. Kobayashi, R., Ishida, S. & Iwamoto, T. An isolable silicon analogue of a ketone that contains an unperturbed Si=O double bond. *Angew. Chem. Int. Ed.* **58**, 9425–9428 (2019).
20. Li, L. et al. Germanone as the first isolated heavy ketone with a terminal oxygen atom. *Nat. Chem.* **4**, 361–365 (2012).
21. Wang, Y. et al. Splitting molecular oxygen en route to a stable molecule containing diphosphorus tetroxide. *J. Am. Chem. Soc.* **135**, 19139–19142 (2013).
22. Huber, F., Westhoff, T. & Preut, H. Tris(2,4,6-trimethylphenyl) antimony dihydroxide; synthesis and reaction with sulfonic acids RSO_3H ($R = C_6H_5$, CF_3). Crystal structure of $[2,4,6\text{-}(CH_3)_3C_6H_2]_3SbO\cdot HO_3SC_6H_5$. *J. Organomet. Chem.* **323**, 173–180 (1987).
23. Wenger, J. S. & Johnstone, T. C. Unsupported monomeric stibine oxides (R_3SbO) remain undiscovered. *Chem. Commun.* **57**, 3484–3487 (2021).
24. Wenger, J. S., Wang, X. & Johnstone, T. C. H-atom assignment and Sb–O bonding of $[Mes_3SbOH][O_3SPh]$ confirmed by neutron diffraction, multipole modeling, and Hirshfeld atom refinement. *Inorg. Chem.* **60**, 16048–16052 (2021).
25. Egorova, I. V., Zhidkov, V. V., Grinishak, I. P. & Rodionova, N. A. Novel organoantimony compounds $[2,6\text{-}(OMe)_2C_6H_3]_3SbO$ and $[2,6\text{-}(OMe)_2C_6H_3]_3Sb(NCO)_2\cdot 0.5(CH_3)_2CO$. *Synthesis and structure. Russ. J. Gen. Chem.* **86**, 2484–2491 (2016).
26. Sasaki, S., Sutoh, K., Murakami, F. & Yoshifuji, M. Synthesis, structure and redox properties of the extremely crowded triarylpnictogens: tris(2,4,6-triisopropylphenyl)phosphine, arsine, stibine and bismuthine. *J. Am. Chem. Soc.* **124**, 14830–14831 (2002).
27. Sasaki, S., Sutoh, K., Shimizu, Y., Kato, K. & Yoshifuji, M. Oxidation of tris(2,4,6-triisopropylphenyl)phosphine and arsine. *Tetrahedron Lett.* **55**, 322–325 (2014).
28. Westhoff, T., Huber, F., Rüther, R. & Preut, H. Synthesis and structural characterization of some new triorganoantimony oxides. Molecular and crystal structure of tris(2,4,6-trimemethylphenyl)antimony dihydroxide. *J. Organomet. Chem.* **352**, 107–113 (1988).
29. Lindquist-Kleissler, B., Weng, M., Le Magueres, P., George, G. N. & Johnstone, T. C. Geometry of pentaphenylantimony in solution: support for a trigonal bipyramidal assignment from X-ray absorption spectroscopy and vibrational spectroscopic data. *Inorg. Chem.* **60**, 8566–8574 (2021).
30. Kleemiss, F. et al. Accurate crystal structures and chemical properties from NoSpherA2. *Chem. Sci.* **12**, 1675–1692 (2021).
31. Desiraju, G. R. Hydrogen bridges in crystal engineering: interactions without borders. *Acc. Chem. Res.* **35**, 565–573 (2002).
32. Bader, R. F. W. A quantum theory of molecular structure and its applications. *Chem. Rev.* **91**, 893–928 (1991).
33. Lindquist-Kleissler, B., Wenger, J. S. & Johnstone, T. C. Analysis of oxygen-pnictogen bonding with full bond path topological analysis of the electron density. *Inorg. Chem.* **60**, 1846–1856 (2021).
34. Pan, B. & Gabbaï, F. P. $[Sb(C_6F_5)_4][B(C_6F_5)_4]$: an air stable, Lewis acidic stibonium salt that activates strong element-fluorine bonds. *J. Am. Chem. Soc.* **136**, 9564–9567 (2014).
35. Bhat, K. L., Markham, G. D., Larkin, J. D. & Bock, C. W. Thermodynamics of boroxine formation from the aliphatic boronic acid monomers $R\text{–}B(OH)_2$ (R=H, H_3C, H_2N, HO and F): a computational investigation. *J. Phys. Chem. A* **115**, 7785–7793 (2011).

Data availability

All the data underlying the findings of this study are available in this Article and its Supplementary Information. All the crystallographic data for the structures reported in this Article have been deposited at the Cambridge Crystallographic Data Centre, under deposition numbers CCDC 2133036 (**1a**), 2182475 (**1b**), 2182476 (**1c**), 2182474 (**2a** orthorhombic), 2133037 (**2a** monoclinic), 2182477 (**2b**), 2182478 (**2c**), 2133038 (**3**), 2182479 (**4**), 2133039 (**5**), 2182480 (**6** triclinic), 2182481 (**6** rhombohedral), 2133040 (**7a**), 2182482 (**7b**), 2133041 (**8**) and 2133042 (**9**). Copies of the data can be obtained free of charge via https://www.ccdc.cam.ac.uk/structures/. Source data used to generate graphs in Figs. 4 and 5, as well as Supplementary Figs. 75, 85–88 and 96, are available as Supplementary Data files. The Cartesian coordinates of all computationally optimized molecular structures are provided in Supplementary Tables 19–31 and are also provided as Supplementary Data. Source data are provided with this paper.

Acknowledgements

The single-crystal X-ray diffractometer housed in the UCSC X-ray Diffraction Facility was funded by the National Science Foundation (2018501 to T.C.J.). This work was additionally supported by a CAREER award from the National Science Foundation (2236365 to T.C.J.). Use of the Stanford Synchrotron Radiation Lightsource (SSRL), SLAC National Accelerator Laboratory, is supported by the US Department of Energy (DOE), Office of Science, Office of Basic Energy Sciences under contract no. DE-AC02-76SF00515, the SSRL Structural Molecular Biology Program is supported by the DOE Office of Biological and Environmental Research, and by the National Institutes of Health, National Institute of General Medical Sciences (including P41GM103393 and P30GM133894). The 800-MHz NMR spectrometer at UCSC was funded by the Office of the Director, NIH, under High End Instrumentation (HEI) grant no. S10OD018455. G.N.G. acknowledges support from a Canada Research Chair and the Natural Sciences and Engineering Research Council of Canada. The funders had no role in study design, data collection and analysis, decision to publish or preparation of the manuscript. We thank M. Qureshi (SSRL) for assistance with remote access data collection during the COVID-19 pandemic.

Author contributions

J.S.W., G.N.G. and T.C.J. designed the experiments. J.S.W. conducted the experiments. J.S.W., M.W., G.N.G. and T.C.J. analysed data. J.S.W., G.N.G. and T.C.J. prepared the manuscript.

Competing interests

The authors declare no competing interests.

Additional information

Supplementary information The online version contains supplementary material available at https://doi.org/10.1038/s41557-023-01160-x.

Correspondence and requests for materials should be addressed to Timothy C. Johnstone.

Peer review information *Nature Chemistry* thanks Martyn Coles, Cem (B.) Yildiz and the other, anonymous, reviewer(s) for their contribution to the peer review of this work.

Reprints and permissions information is available at www.nature.com/reprints.